Photostable Iodinated Silica/Porphyrin Hybrid Nanoparticles with Heavy-Atom Effect for Wide-Field Photodynamic/ Photothermal Therapy Using Single Light Source

Koichiro Hayashi, Michihiro Nakamura, Hirokazu Miki, Shuji Ozaki, Masahiro Abe, Toshio Matsumoto, Toshinari Kori, and Kazunori Ishimura*

Physical therapies including photodynamic therapy (PDT) and photothermal therapy (PTT) can be effective against diseases that are resistant to chemotherapy and remain as incurable malignancies (for example, multiple myeloma). In this study, to enhance the treatment efficacy for multiple myeloma using the synergetic effect brought about by combining PDT and PTT, iodinated silica/porphyrin hybrid nanoparticles (ISP HNPs) with high photostability are developed. They can generate both $^1O_2$ and heat with irradiation from a light-emitting diode (LED), acting as photosensitizers for PDT/PTT combination treatment. ISP HNPs exhibit the external heavy atom effect, which significantly improves both the quantum yield for $^1O_2$ generation and the light-to-heat conversion efficiency. The in vivo fluorescence imaging demonstrates that ISP HNPs, modified with folic acid and polyethylene glycol (FA-PEG-ISP HNPs), locally accumulate in the tumor after 18 h of their intravenous injection into tumor-bearing mice. The LED irradiation on the tumor area of the mice injected with FA-PEG-ISP HNPs causes necrosis of the tumor tissues, resulting in the inhibition of tumor growth and an improvement in the survival rate.

1. Introduction

Physical therapies using nanoparticles can be effective against diseases such as multiple myeloma, which is resistant to chemotherapy and remains an incurable malignancy.[1] Physical therapy includes photodynamic therapy (PDT) and photothermal therapy (PTT).[2,3]

PDT is a form of phototherapy that uses a photosensitizer (PS), which is exposed to light at a diseased site. On exposure to light, singlet oxygen ($^1O_2$), the main cytotoxic reactive oxygen species, is generated, which causes death of diseased cells.[2] $^1O_2$ is produced by excitation of PS to its triplet state on exposure to light and by the subsequent transfer of the energy to ground state of the surrounding molecular oxygen. It is necessary for PS to have an absorption peak at wavelengths ranging from 600 to 800 nm, i.e. the near-infrared window, because light with wavelengths within this window penetrates deeply into living tissues and generates $^1O_2$. Light with wavelengths in the range 800–900 nm also penetrates deep into the tissue; however, very little $^1O_2$ is obtained when the absorption peak of PS is above the wavelength of 800 nm because the photoexcited triplet state of PS falls below the excited state of $^1O_2$ (94 kJ/mol). PDT is a local treatment and has few side effects when compared to conventional chemotherapies and radiotherapies. However, PS gradually decays by light irradiation.[4] Additionally, as soon as PDT is performed, severe local hypoxia is caused by both consumption of tissue oxygen and reduction in oxygen supply cause by the damage of blood vessels and eventually, the production of $^1O_2$ ceases.[5–9] These issues hinder the therapeutic efficacy of PDT and greatly restrict its potential applications in the clinic. Therefore, to overcome the intrinsic limitations of PDT, a new strategy is required to improve the therapeutic index upon prolonged light irradiation.

PTT is a hyperthermia treatment that uses heat, which is obtained by the conversion of energy absorbed from photons by the PS.[3] Hyperthermia, commonly defined as heating of tissue in the range 41–47 °C for tens of minutes, causes irreversible

Dr. K. Hayashi, Dr. M. Nakamura, Prof. K. Ishimura
Department of Anatomy and Cell Biology
Institute of Health Biosciences
The University of Tokushima Graduate School
3–18–15 Kuramoto-cho, Tokushima, 770–8503, Japan
E-mail: hayashi@tokushima-u.ac.jp
Dr. H. Miki
Division of Transfusion Medicine
Tokushima University Hospital
2–50–1 Kuramoto-cho, Tokushima, 770–0042, Japan

DOI: 10.1002/adfm.201301771

Dr. S. Ozaki
Department of Internal Medicine
Tokushima Prefectural Central Hospital
1–10–3 Kuramoto-cho, Tokushima, 770–0042, Japan
Dr. M. Abe, Prof. T. Matsumoto
Department of Medicine and Bioregulatory Sciences
The University of Tokushima Graduate School
of Medical Sciences 3–18–15 Kuramoto-cho, Tokushima, 770–8503, Japan
Dr. T. Kori
Tokushima Prefectural Industrial Technology Center
11–2 Nishibari, Saigacho, Tokushima, 770–8021, Japan

cell damage by loosening of cell membranes, denaturation of proteins, and eventually leads to destruction of the diseased tissue.[10] PTT treats even hypoxic tissues because it does not require oxygen. However, similar to PDT, the drawback of PTT is that the PS is destroyed with time during light irradiation and resulting eventually in the generation of very little heat.

The combination of PDT and PTT can lead to a synergistic effect. To obtain the synergistic effect, most previous studies developed a PS for PDT/PTT combination treatment by incorporating separate PSs for PDT and PTT.[11,12] Unfortunately, the absorption bands of these PSs were mismatched within the near-infrared window.[13] Therefore, two light sources of different wavelengths were used, and PDT and PTT were separately carried out. This sequential irradiation complicates the treatment process and it is difficult to focus the two light beams at the same position. The development of a PS that generates both $^1O_2$ and heat by irradiation with a light source of single wavelength can enable PDT/PTT combination treatment continuously and simultaneously, leading to the synergistic effect and enhancement of the therapeutic efficacy.

Lasers have been used as light sources for PDT and PTT; however, the excessive laser power rapidly destroy the PSs. Hence, the PSs become non-functional within a short time. Moreover, therapies with laser are available only when the location of cancer is identified. Diffuse, poorly demarcated, and metastatic cancer is difficult to treat using lasers because the spot size i.e., the irradiation area of the laser is small. In addition, high power lasers used for treatment need large installation space and high costs. However, the use of light-emitting diodes (LED) instead of lasers can delay the destruction of the PSs because the power ratings of LEDs are much lower than lasers. Furthermore, LEDs can irradiate extensively, and therefore, therapies with LEDs can treat diffuse, poorly demarcated, and metastatic cancers. Additionally, LEDs have high light conversion efficiencies, long service lives, and are more compact and economical than lasers. Hence, to achieve PDT/PTT combination treatment using LEDs, a PS generating $^1O_2$ and heat with high efficiencies even under low-power irradiation needs to be developed.

Porphyrins are potentially good candidates as PSs that can be used in PDT/PTT combination treatment because they effectively yield $^1O_2$ by light irradiation and they have been already used as clinical PSs for PDT.[14–16] However, their light-to-heat conversion (LHC) efficiency is relatively low within the near-infrared window because their absorption bands at wavelengths ranging from 500 to 700 nm, called Q bands, are intrinsically forbidden and they exhibit low absorption of light. Metal nanoparticles such as gold nanorods (Au NRs) are promising PSs for PTT because they can convert light energy into heat within this window. However, they cannot yield $^1O_2$ on light exposure, and therefore they are unusable as PSs for PDT. In addition, they show poor photostability and melt under light irradiation, which are serious disadvantages.[17–19] Hence, they progressively lose the light absorption ability within the near-infrared window and their ability to generate heat reduces. Dye-type PSs including porphyrins also suffer this drawback of low photostability. Nevertheless, their photostability is significantly improved by their encapsulation in silica matrices.[20–22] From the above discussion, it is clear that the enhancement of the LHC efficiency of porphyrins is a key issue, and the photostability can be improved by encapsulating the porphyrin in a silica matrix. If porphyrins gain both high LHC efficiency within the near-infrared window and high photostability, they can be applied as a PS for PDT/PTT combination treatment using LEDs as a single light source.

The spin-orbit coupling of a PS is enhanced within matrices containing heavy atoms, which weakens spin prohibition. This is known as the external heavy atom effect.[23] Therefore, by employing this effect, the spin prohibition of Q bands of porphyrins can be overcome, leading to an increase in their absorbances. As a result, the LHC efficiency of porphyrins can be improved within the near-infrared window to enhance the effect of PTT. In addition, the heavy atom effect promotes the intersystem crossing (ISC) from the photoexcited singlet of the PS to the photoexcited triplet state, leading to an improvement in the $^1O_2$ yield. Hence, the effect of PDT can be enhanced. So far, Prasad et al. have demonstrated that encapsulating the PS in iodine-containing silica nanoparticles increases the $^1O_2$ production by the external heavy atom effect, resulting in the improvement of the in vitro PDT efficacy.[24] However, curiously, the normalized absorbance did not increase; instead, the normalized absorbance decreased, indicating that the LHC efficiency was not improved. Therefore, the nanoparticles are difficult to be used as PSs for PTT. In addition, it has been reported that densely packing the porphyrins in nanoparticles (>8000 molecules per particle) enhances the LHC efficiency, and the nanoparticles increase the temperature by more than three times when compared with monomeric porphyrins.[25,26] From the above discussion, it can be understood that both the heavy atom effect and densely encapsulating porphyrins in silica nanoparticles are effective for the enhancement of the LHC efficiency.

Encapsulating porphyrins in silica nanoparticles governs both the content of porphyrins in the silica nanoparticles and the leakage of porphyrins from silica nanoparticles.[27] In most cases, porphyrins are not well encapsulated in silica nanoparticles by physical entrapment within the siloxane network because of their large size. As an exception, the emulsion method successfully encapsulates porphyrins in silica nanoparticles.[24] However, this method needs to use a toxic surfactant, dioctyl sodium sulfosuccinate, which is a strong eye, lung, and skin irritant and causes diarrhea, intestinal bloating, and occasionally cramping pains.[28] This method also needs long periods of dialysis for purification. Furthermore, in the case of the physical entrapment, porphyrins leak from the siloxane network and cause side effects.[27] Covalent inclusion of porphyrins in silica nanoparticles is expected to overcome these drawbacks.[29,30] We have successfully synthesized in a single step silica nanoparticles with high porphyrin content via covalent linkage by a sol-gel method using a porphyrin-containing silicon alkoxide (PCSA) as a precursor, without using surfactants.[31–34]

Based on our previous study, we have, in the present study, synthesized iodinated silica nanoparticles with high porphyrin content via covalent linkage, i.e., iodinated silica/porphyrin (ISP) hybrid nanoparticles (HNPs), by a sol-gel method using PCSA and (3-iodopropyl)trimethoxysilane (IPTMS) as precursors. As a control material, non-iodinated silica nanoparticles

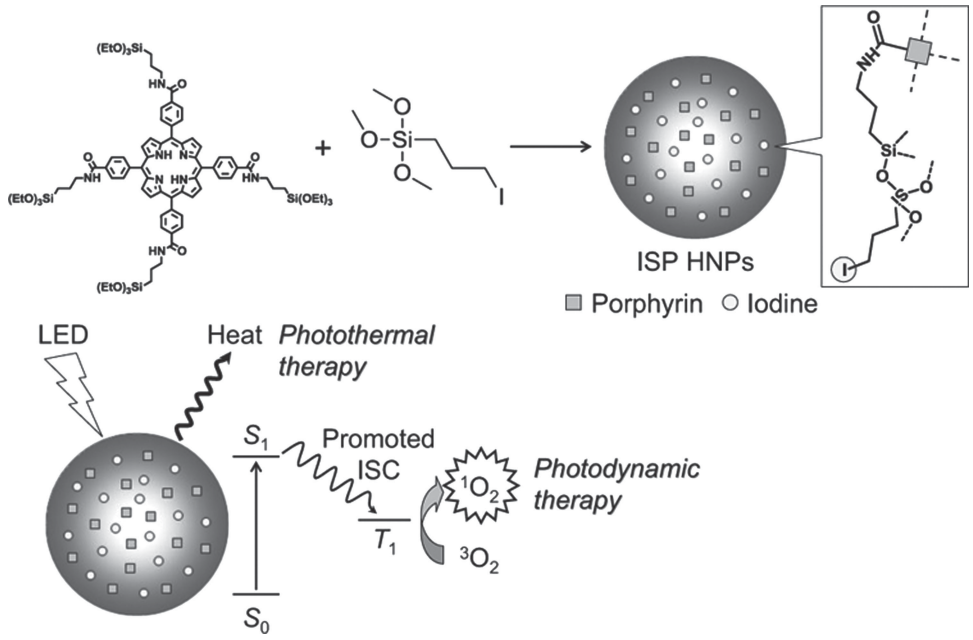

Figure 1. Synthesis scheme of ISP HNPs (upper). Illustration of PDT/PTT combination therapy by the enhancement of $^1O_2$ generation via promotion of ISC using the heavy atom effect and the conversion of the energy absorbed from photons into heat (lower).

containing porphyrin, i.e., silica/porphyrin (SP) HNPs, were produced by a method similar to the synthesis used for the production of ISP HNPs by using tetraethyl orthosilicate (TEOS) instead of IPTMS. The expression of the external atom effect was confirmed by comparing the normalized absorbance between ISP HNPs and SP HNPs. To assess the effectiveness of the external heavy atom effect, we compared the $^1O_2$ generation efficiency and photothermal efficiency between ISP HNPs and SP HNPs. The usefulness of ISP HNPs as PSs for PDT/PTT combination treatment was estimated by comparing the $^1O_2$ generation efficiencies, photothermal efficiencies, and photostabilities of ISP HNPs, SP HNPs, typical PSs, and Au NRs. Furthermore, we evaluated the in vivo efficacy of the PDT/PTT combination treatment for multiple myeloma using ISP HNPs as PSs and an LED as a single light source.

2. Results and Discussion

ISP HNPs were synthesized via the sol-gel reaction using PCSA and IPTMS as precursors and ammonia water as a catalyst (**Figure 1**). In most cases, the sol-gel reaction only using trifunctional alkoxysilanes as precursors, by not using tetrafunctional alkoxysilanes, involves multistep hydrolysis-condensation processes or the use of surfactants. However, ISP HNPs were formed via a single-step hydrolysis-condensation process of trifunctional alkoxysilanes, IPTMS, and PCSA, without any surfactants. As a control material, SP HNPs were synthesized by a similar method using TEOS instead of IPTMS.

As shown in the transmission electron microscopy (TEM) images, ISP HNPs were comparatively monodisperse (**Figure 2**A), and occurred as spheres with rough surfaces (Figure 2B). Their mean diameter, as estimated from the TEM images, was 47 ± 12 nm (Figure 2C). SP HNPs were also comparatively monodisperse (Figure S1A) and of a shape to similar to that of ISP HNPs (Figure S1B). The mean diameter of the SP HNPs was 42 ± 10 nm (Figure S1C).

The two resonance peaks at –59.5 ppm and –68.3 ppm in the solid state ^{29}Si nuclear magnetic resonance (NMR) spectrum of the ISP HNPs (Figure 2D), could be ascribed to the Si environments of T^2 and T^3, respectively.[35–37] These results established that two or three of the alkoxy groups of PCSA and IPTMS underwent hydrolysis and condensation to form a siloxane network. The peak 1 at 119.1 ppm and the peak 2 at 128.9 ppm in the solid state ^{13}C NMR spectra of ISP HNPs (Figure 2E) were assigned to pyrrole rings in porphyrin.[38,39] The peak 4 at 145.6 ppm and the peak 5–7 at 134.0 ppm were attributed to aromatic rings in porphyrin. The peak 8 at 164.1 ppm was due to the carbon of the amide. The peak 9 at 37.7 ppm, the peak 10 at 23.6 ppm, and the peak 11 at 11.3 ppm were identified as the C^9, C^{10}, and C^{11} of $SiC^{11}C^{10}C^9NHCOR$, respectively. The peak 12 at 17.0 ppm, the peak 13 at 32.3 ppm, and the peak 14 at 41.4 ppm were assigned to the C^{12}, C^{13}, and C^{14} of $SiC^{12}C^{13}C^{14}I$, respectively. These results demonstrated that porphyrin molecules were incorporated into the siloxane network of the ISP HNPs at the molecular level via amide linkage. The solid state ^{29}Si NMR spectrum of SP HNPs showed three resonance peaks at –68.3, –102.2, and –112.5 ppm, which were attributed to the Si environments of T^3, Q^3, and Q^4, respectively (Figure S2A).[35–37] These results revealed that the three alkoxy groups of PCSA and the three or four alkoxy groups of TEOS underwent hydrolysis and condensation to form a siloxane network. The peak 1 at 119.2 ppm and the peak 2 at 124.5 ppm in the solid state ^{13}C NMR spectrum of SP HNPs (Figure S2B) could be ascribed to pyrrole rings in porphyrin.[38,39] The peak 4 at 144.1 ppm and the peak 5–7 at 138.8 ppm were assigned to aromatic rings in

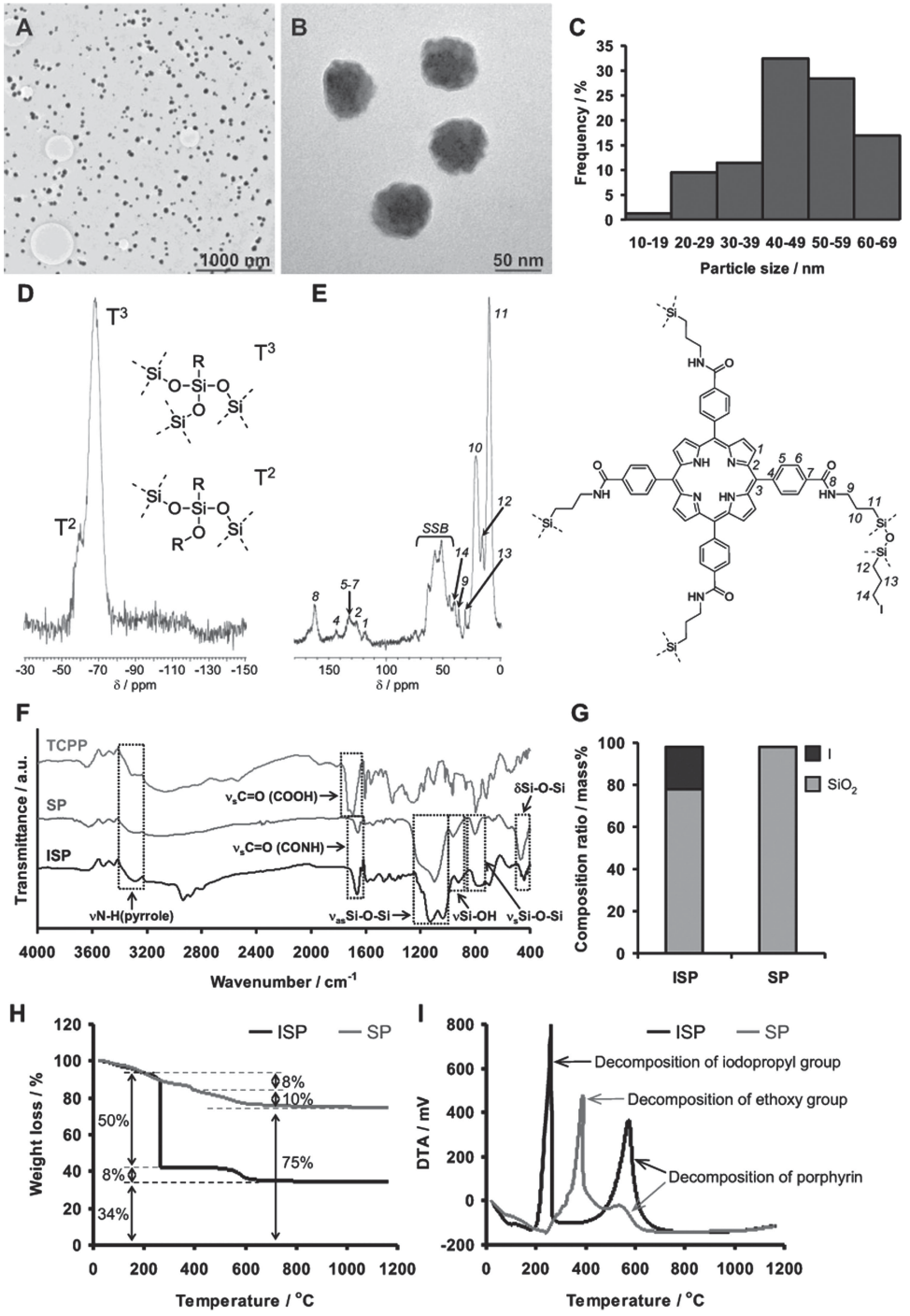

Figure 2. (A) TEM images of ISP HNPs. (B) Magnified image of Fig. 2A. (C) Size distribution of ISP HNPs estimated from the TEM images. Solid state (D) ^{29}Si and (E) ^{13}C NMR spectra of the ISP HNPs. (F) FTIR spectra of TCPP, SP HNPs, and ISP HNPs. (G) Compositions of SP HNPs and ISP HNPs analyzed by XRF. (H) TG and (I) DTA curves of ISP HNPs and SP HNPs.

porphyrin. The peak 8 at 165.3 ppm was assigned to the carbon of the amide. The peak 9 at 36.0 ppm, the peak 10 at 22.7 ppm, and the peak 11 at 9.5 ppm were identified as the C9, C10, and C11 of the SiC^{11}C^{10}C^{9}NHCOR, respectively. These results demonstrated that the SP HNPs consisted of the siloxane network that incorporated porphyrin molecules via an amide linkage similar to the ISP HNPs.

The Fourier transform infrared (FTIR) spectra of TCPP, SP, and ISP showed that the absorptions attributed to the pyrrole rings in the porphyrin appeared at 3430–3250 cm^{-1}

(Figure 2F).[40] In the spectra of ISP HNPs and SP HNPs, the absorptions due to the siloxane bond were present at 1260–1010 cm^{-1}, 870–740 cm^{-1}, and 540–410 cm^{-1}, and a band ascribed to silanol was found at 1005–880 cm^{-1}.[41–43] The absorption attributed to carboxylic acid appeared at 1800–1640 cm^{-1} in the spectrum of TCPP. However, this band disappeared and the absorptions attributed to amide appeared at 1740–1620 cm^{-1} in the spectra of ISP HNPs and SP HNPs. These findings revealed that the porphyrin molecules were incorporated in the siloxane network of ISP HNPs and SP HNPs via amide linkages.

The X-ray fluorescence spectroscopic (XRF) analysis of the ISP HNPs demonstrated that the mass ratio of iodine to that of silica within was 0.25 (Figure 2G). In the SP HNPs, iodine was absent.

In the thermogravimetric (TG) curve of ISP HNPs (Figure 2H), the weight losses of 7% below 200 °C, 51% at 200–280 °C, and 8% at 490–680 °C appeared, and the residue was 34%. In the differential thermal analysis (DTA) curve of the ISP HNPs (Figure 2I), one endothermic peak was observed around 100 °C, and two exothermic peaks were seen at 260 °C and 580 °C. The endothermic peak was caused by the dehydration of adsorbed water and the exothermic peaks were attributed to the decomposition of iodopropyl group and porphyrin, respectively.[44–46] These results demonstrated that the ISP HNPs consisted of 7% of adsorbed water, 51% of iodopropyl group, 8% of porphyrin, and 34% of silica. From this, the ISP HNPs contained in 0.13 mmol of porphyrin per gram, or the porphyrin packing density was >9300 molecules per particle. The TG curve of the SP HNPs showed weight losses of 7% below 200 °C, 8% at 200–410 °C, and 10% at 410–680 °C, and the residue was 75%. In the DTA curve of the SP HNPs, the endothermic peak at around 100 °C could be ascribed to the dehydration of adsorbed water, and the exothermic peaks present at 390 °C and 560 °C could be attributed to the decomposition of ethoxy groups and porphyrin, respectively.[44–46] These results revealed that the SP HNPs consisted of 7% of adsorbed water, 8% of ethoxy groups, 10% of porphyrin, and 75% of silica. From this, the SP HNPs contained in 0.16 mmol of porphyrin per gram, or the porphyrin packing density was found to be >8100 molecules per particle.

The ultraviolet–visible (UV–vis) spectra showed that the absorbance of Q bands by TCPP and SP HNPs was very low, because Q bands were inherently spin-prohibited (**Figure 3**A). However, ISP HNPs showed significantly higher Q band absorbance than SP HNPs and TCPP, indicating that the spin prohibition of Q bands in ISP HNPs was overcome by the external heavy atom effect. The ratios of the absorbance at 650 nm (A_{650}) to the absorbance of the Soret band (A_{Soret}) of ISP HNPs, SP HNPs, and TCPP were 0.168, 0.058, and 0.008, respectively (Figure 3B). A comparison of the A_{650}/A_{Soret} of the ISP HNPs and SP HNPs demonstrated that the external heavy atom effect increased the light absorption by about three-fold. In addition, the A_{650}/A_{Soret} of SP HNPs was about seven times larger than that of TCPP, indicating that incorporating porphyrin molecules in silica nanoparticles contributed to the increase in light absorption. Zheng et al. reported that nanoparticles containing a high concentration of porphyrin molecules (>8000 molecules per particle) absorb light with extremely high efficiency compared to monomeric porphyrins. As estimated from TG-DTA, the porphyrin packing densities in ISP HNPs and SP HNPs were more than 9300 and 8100 molecules per particle, respectively. From the above findings, in addition to the external heavy atom effect, the condensation of porphyrin molecules into silica nanoparticles also made a significant contribution to the enhancement of the light absorption of ISP HNPs.

The $^1O_2$ generated from ISP HNPs, SP HNPs, and TCPP under light irradiation was detected using the chemical trapping reagent 1,3-diphenylisobenzofuran (DPBF). DPBF reacts with $^1O_2$ irreversibly, undergoing a 1,4-cycloaddition, which is detected as a decrease in the intensity of the DPBF absorption band at 410 nm.[47] As shown in Figure 3C, the absorbance of the solution containing ISP HNPs and DPBF decreased gradually as a function of time under light irradiation using a LED with a peak wavelength of 650 nm at 5 mW/cm^2 and a spot size of 22 mm. The relative quantum yield for $^1O_2$ generation (Φ_Δ) was determined using a comparative method. A plot of optical absorbance at 410 nm as a function of the irradiation time was consistent with a first order reaction (Figure 3D). The Φ_Δ was calculated by comparison with a standard PS, methylene blue (MB),[48]

$$\Phi_\Delta = \Phi_S(k/I)\ (I_S/k_S)$$

where k and k_S are the rate constants for decomposition of DPBF by ISP HNPs, SP HNPs, or TCPP and by MB, respectively. I and I_S represent light absorbed by ISP HNPs, SP HNPs, or TCPP and by MB, respectively, which were determined by integration of the optical absorption bands in the wavelength range 455–500 nm. As shown in Figure 3E, Φ_Δ of ISP HNPs was 1.5 times higher than that of SP HNPs; further, the Φ_Δ of SP HNPs was 1.1 times as high as that of TCPP. These results demonstrated that the heavy atom effect significantly enhanced the generation efficiency of $^1O_2$, which was also marginally enhanced by the incorporation of the porphyrin molecules in silica nanoparticles. In addition to the heavy atom effect, the condensation of porphyrin molecules into silica nanoparticles also led to an increase in light absorption, as described above. Furthermore, the Φ_Δ of ISP HNPs was higher than that of typical and clinical PSs. Thus, ISP HNPs can be useful as PSs for PDT.[49–51]

To assess the LHC efficiency of ISP HNPs, we irradiated an aqueous solution containing ISP HNPs with the LED and monitored the solution temperature using thermography. For comparison, the LHC efficiencies of SP HNPs, TCPP, Au NRs, and water were also evaluated by similar methods. Figure S3 shows the infrared images of these solutions exposed to the LED light for 20 min. ISP HNPs significantly increased the solution temperature compared to SP HNPs, demonstrating that the heavy atom effect exerted a strong positive effect on the enhancement of LHC efficiency, which was attributed to the increase in light absorption. Nevertheless, SP HNPs also raised the solution temperature, although the TCPP solution too contributed a little to its increase in temperature. These results confirmed that condensing porphyrin molecules into silica nanoparticles also improved the LHC efficiency. Thus, both the heavy atom effect and the condensation of porphyrin molecules into silica nanoparticles were beneficial to the enhancement of LHC efficiency in addition to $^1O_2$ generation. Moreover, the temperature of the

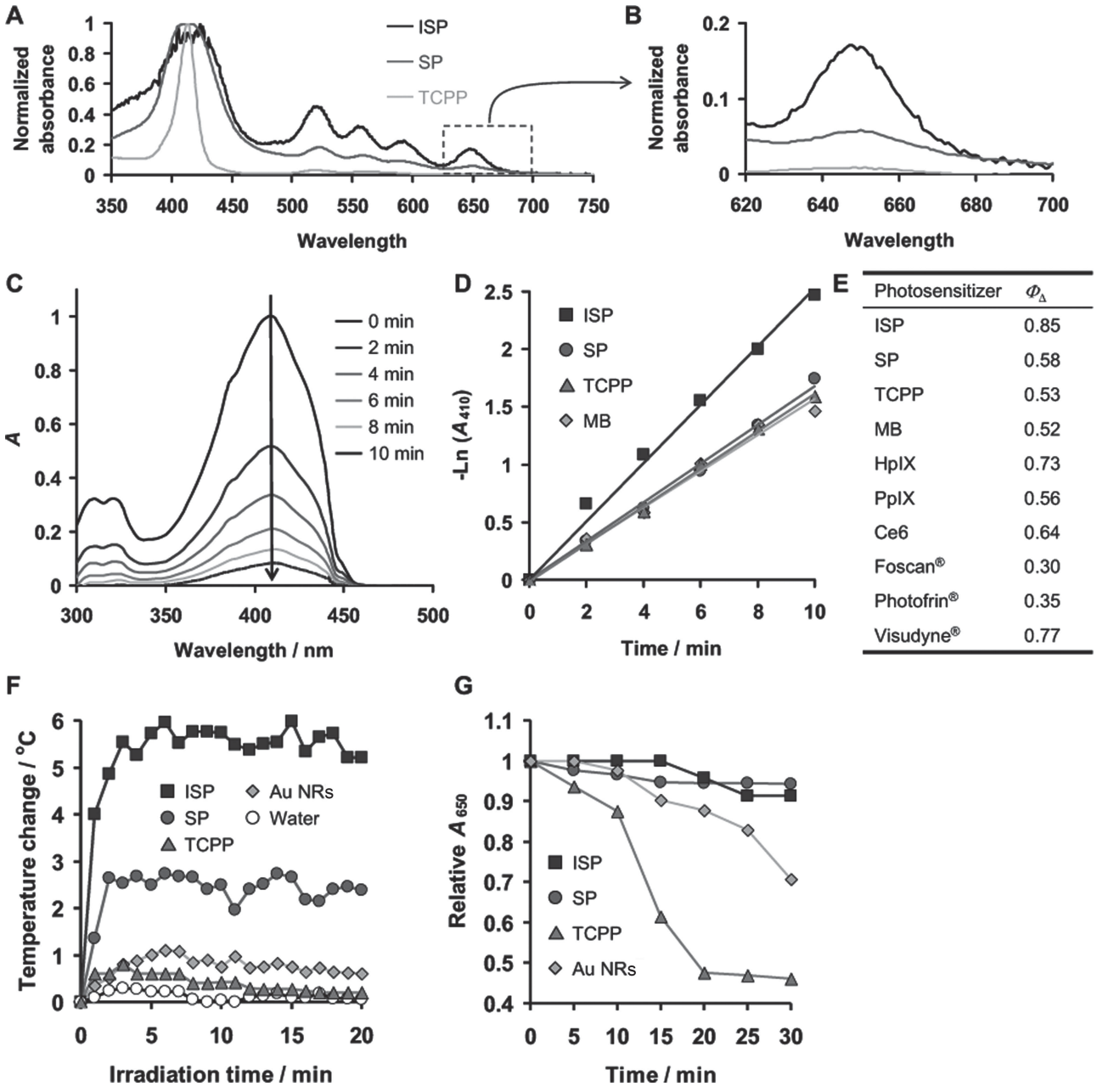

Photosensitizer	Φ_Δ
ISP	0.85
SP	0.58
TCPP	0.53
MB	0.52
HpIX	0.73
PpIX	0.56
Ce6	0.64
Foscan®	0.30
Photofrin®	0.35
Visudyne®	0.77

Figure 3. (A) UV–vis absorption spectra of ISP HNPs, SP HNPs, and TCPP. (B) Magnified image of the region enclosed by the dotted line in Fig. 3A. (C) UV-Vis absorption spectra of the solution containing DPBF and ISP HNPs exposed to LED light for 0–10 min. (D) Changes in absorbance of the solution containing DPBF and ISP HNPs, SP HNPs, TCPP, or MB with irradiation time at a wavelength of 410 nm. (E) Φ_Δ of ISP HNPs, SP HNPs, TCPP, MB, and typical PSs (HpIX: hematoporphyrin IX, PpIX: protoporphyrin IX, Ce6: chlorin e6, Foscan: meta(tetrahydroxyphenyl)chlorin, Photofrin®: porfimer sodium, Visudyne: verteporfin). (F) Temperature changes of ISP HNPs, SP HNPs, TCPP, Au NRs, and water with irradiation time. (G) Photostability of ISP HNPs, SP HNPs, TCPP, and Au NRs under LED light irradiation estimated from the change in absorbance at a wavelength of 650 nm.

Au NRs solution was higher than that of the TCPP solution, but was lower than that of the SP HNPs solution. Water changed little in temperature because of the light irradiation. The temperature changes of these solutions were plotted every 1 min for 20 min, as shown in Figure 3F. The temperature of the solutions containing ISP HNPs, SP HNPs, TCPP, and Au NRs increased by 6.0, 2.7, 0.8, and 1.1 °C, respectively. The TCPP and Au NRs solutions reached the maximum temperature at 3 min and 6 min, respectively, and then their temperature decreased. In contrast, the temperatures of the ISP HNPs and SP HNPs solutions were maintained near the maximum temperature. To investigate the causes for this observation, we assessed the photostabilities of ISP HNPs, SP HNPs, TCPP, and Au NRs by monitoring the changes of A_{650} during the LED irradiation (Figure 3G). The relative A_{650} of TCPP dramatically decreased immediately after the LED irradiation to

0.46 after 30 min. The relative A_{650} of Au NRs was constant for the first 5 min and then gradually decreased to 0.70 after 30 min because Au NRs melted by the 30 min LED irradiation, as shown in the TEM images (Figure S4A). These findings demonstrated that the photodegradation of TCPP and Au NRs caused the decrease in temperature of the solutions containing TCPP and Au NRs. However, the reductions in the relative A_{650} values of the ISP HNPs and SP HNPs were limited. As shown in the TEM images (Figure S4B), ISP HNPs exposed to the LED for 30 min remained unchanged in form when compared to their state before irradiation. Thus, ISP HNPs and SP HNPs possessed relatively high photostabilities. The above results demonstrate that encapsulating porphyrin molecules into silica nanoparticles improved the photostability, and furthermore, the improvement of photostability led to a stable heat generation.

The effective delivery of ISP HNPs to tumors is imperative for PDT/PTT combination treatment. The surface modification of ISP HNPs with polyethylene glycol (PEG), known as PEGylation, inhibits phagocytosis by the reticuloendothelial system (RES) and prolongs the retention time in blood.[52] These factors promote the enhanced permeability and retention (EPR) effect.[53] Folic acid (FA) binds to folate receptors, which are overexpressed in various types of human cancer cells.[54] However, these are, in general, absent in most normal cells. Therefore, the surface modification of ISP HNPs with FA increases their accumulation in tumors. From these reasons, we modified ISP HNPs with FA and PEG by the following protocol. First, the ISP HNPs were functionalized with thiol groups by the hydrolysis-condensation of 3-mercaptopropyl(dimethoxy) methylsilane (MPDMMS). Then, the thiol-functionalized ISP HNPs (SH-ISP HNPs) were coupled to PEG and FA via the reaction between thiol and maleimide (Mal) using FA and Mal-heterobifunctionalized PEG (FA-PEG-Mal).

The zeta potentials of ISP HNPs, SH-ISP HNPs and FA- and PEG-modified ISP HNPs (FA-PEG-ISP HNPs) were –0.96, 4.78 and –0.10 mV, respectively, in phosphate buffered saline (PBS, pH 7.4) as shown in Table S1. The hydrodynamic diameters of ISP HNPs, SH-ISP HNPs and FA-PEG-ISP HNPs were 1880 ± 366 nm, 592 ± 97 nm and 72 ± 14 nm, respectively, in PBS (Figure S5A). The ISP HNPs were aggregated in PBS. The dispersibility of SH-ISP HNPs was slightly better than that of ISP HNPs because the absolute value of zeta potential was increased by the thiol-functionalization of ISP HNPs. The surface modification with PEG and FA led to the decrease in the hydrodynamic diameter, indicating the improvement of the dispersibility in PBS. The hydrodynamic diameter of FA-PEG-ISP HNPs was about 20 nm larger than the particle size of ISP HNPs estimated from TEM images (Figure 2A–C) because FA and PEG were grafted on the particle surface. Furthermore, the hydrodynamic diameter of FA-PEG-ISP HNPs was unchanged for a week after their synthesis (Figure S5B), demonstrating that the FA-PEG-ISP HNPs were stable in PBS for a long period.

We quantified the amount of thiol on the surface of SH-ISP HNPs by use of the thiol specific reagent 4-dithiodipyridine (4-DPS), which reacts with thiol to form stoichiometric amount of the chromogenic compound 4-thiopyridone (4-TP), absorbing at 324 nm.[55] We added 4-DPS solution to SH-ISP HNPs suspension. After reaction, we collected the supernatant by centrifugation and measured its absorbance at 324 nm (A_{324}) due to 4-TP in the supernatant. The amount of thiol per gram of SH-ISP HNPs (c_{SH}) was estimated using the following equation:

$$c_{SH} = A_{324}/(\varepsilon_{324} L m),$$

where ε_{324} is the molar absorbance coefficient of 4-TP at 324 nm (19800 $M^{-1}cm^{-1}$), L is the light path (0.1 cm) and m is the concentration of SH-ISP HNPs (5.42 g/L). Because the A_{324} was 0.086 (see Figure S6), the c_{SH} was estimated to be 8.0 μmol/g. Furthermore, we estimated the amount of FA grafted on the surface of FA-PEG-ISP HNPs from the absorbance at 283 nm (A_{283}) due to p-aminobenzoic acid of FA (Figure S7A). The amount of FA grafted on the surface of FA-PEG-ISP HNPs was estimated to be 7.1 μmol/g based on the calibration curve (Figure S7B), because the A_{283} of FA-PEG-ISP HNPs solution (2.7 mg/mL) was 0.10 (Figure S7C).

To investigate the biodistribution of FA-PEG-ISP HNPs, we injected them intravenously into RPMI8226 tumor-bearing mice and obtained in vivo fluorescence images using IVIS at preinjection and 1 h, 6 h, and 18 h post-injection. FA-PEG-ISP HNPs emitted the strongest fluorescence at the wavelength of 720 nm when the excitation wavelength was 640 nm (Figure S8). An hour after injection, the fluorescence was observed throughout the back of the mouse (Figure S9). Six hours after injection, the fluorescence in the back of the mouse became somewhat limited. Eighteen hours after injection, the tumor was seen to locally emit fluorescence in the dorsal and lateral images (**Figure 4**), and parts emitting fluorescence were also found in the abdomen. The fluorescence images of the dissected mouse and the isolated organs demonstrated that the abdominal fluorescence parts were coincident with the stomach

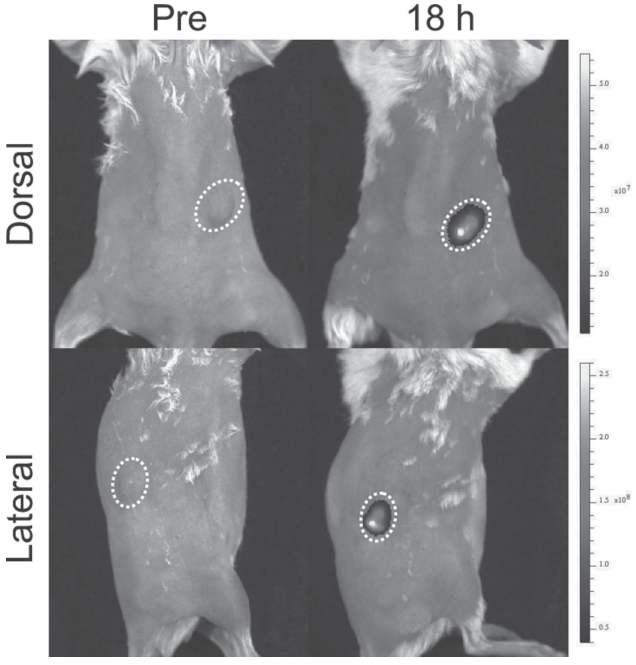

Figure 4. In vivo fluorescence images of the mice before and 18 h after intravenous injection of FA-PEG-ISP HNPs.

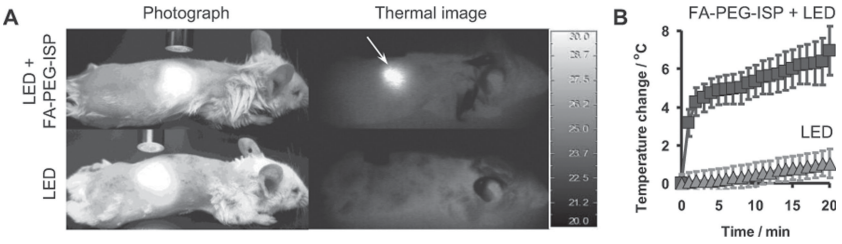

Figure 5. (A) Photographs and thermal images of the mice injected (upper) with and (lower) without FA-PEG-ISP HNPs under LED light irradiation for 20 min. (B) Temperature changes of the tumors of the mice injected with and without FA-PEG-ISP HNPs as a function of irradiation time.

and cecum (Figures S9B and S9C). Furthermore, the tumor emitted the strongest fluorescence among major organs. These results demonstrated that FA-PEG-ISP HNPs accumulated predominantly in the tumor, and a part of them was present in the stomach and cecum.

To confirm whether the FA-PEG-ISP HNPs heated the tumor to a therapeutically effective temperature by the LED irradiation, the tumor areas of the mice injected with and without FA-PEG-ISP HNPs were exposed to the LED light for 20 min. The thermographical measurements revealed that the surface temperature of the tumor of the mice injected with FA-PEG-ISP HNPs locally increased by ~7 °C for 20 min (**Figure 5** and Figure S10). Based on this result, the internal temperature of the tumor was estimated to be ~44 °C, while the body temperature was 37 °C. In contrast, the tumor temperature of mice without injection of FA-PEG-ISP HNPs remained nearly unchanged. Thus, FA-PEG-ISP HNPs converted the energy absorbed from photons to heat, resulting in the rise of the tumor temperature to a therapeutically effective temperature.

The in vivo treatment efficacy of the PDT/PTT combination therapy, using FA-PEG-ISP HNPs and LED light, was assessed by the comparison of the tumor growth in and the survival period between mice exposed to the LED irradiation for 20 min after injection of FA-PEG-ISP HNPs and control mice without treatment, those injected with FA-PEG-ISP HNPs, and those exposed to LED light for 20 min. The tumors of the control mice grew by approximately 25 times in 30 days (**Figure 6**A). Meanwhile, in the mice exposed to the LED irradiation after injection of FA-PEG-ISP HNPs, the tumor growth was significantly inhibited and 30 days after treatment, the tumor volume was one-tenth of that of the control mice. The photographs of the mice 30 days after treatment also demonstrated that the mice exposed to the LED irradiation after injection of FA-PEG-ISP HNPs had appreciably smaller tumors than the control mice (Figures 6C–F). Furthermore, the mice exposed to the LED irradiation after injection of FA-PEG-ISP HNPs were alive after 10 weeks, while the control mice died after up to 7 weeks after treatment (Figure 6B). In addition, the hematoxylin and eosin (H&E) staining of the tumor tissue sections 24 h after treatment revealed that necrotic cell death was extensively caused in the tumor of mice exposed to LED after injection of FA-PEG-ISP HNPs (Figure 6G and Figure S11). However, in the tumor of the control groups, necrotic regions were not observed and viable tumor cells were densely packed (Figures 6H–J). These results demonstrated that the exposure of the tumorous area in mice to LED for 20 min after injection of FA-PEG-ISP HNPs caused necrosis of the tumor tissue, resulting in significant inhibition of tumor growth and improvement of survival rate. From the above findings, FA-PEG-ISP HNPs were found to be promising PSs for the PDT/PTT combination therapy.

3. Conclusion

ISP HNPs were synthesized via a simple sol-gel reaction using PCSA and IPTMS. ISP HNPs effectively yielded $^1O_2$ by LED irradiation (not laser irradiation) because of the external heavy atom effect and their Φ_Δ was higher than typical and currently used clinical PSs. Furthermore, the external heavy atom effect increased the energy of ISP HNPs absorbed from photons. As a result, the ISP HNPs succeeded in heating the tumor to a therapeutically effective temperature under the LED irradiation. Moreover, the exposure of the tumorous area in mice to the LED for 20 min after injection of FA-PEG-ISP HNPs caused necrosis of the tumor tissue, resulting in significant inhibition of the tumor growth and improvement of survival rate. Thus, the PDT/PTT combination therapy with FA-PEG-ISP HNPs can be effective against multiple myeloma, which is resistant to chemotherapy and remains as an incurable malignancy.

4. Experimental Section

Reagents: IPTMS and 1,3-diphenylisobenzofuran (DPBF) were purchased from Sigma-Aldrich (MO, USA). Tetrakis(4-carboxyphenyl)porphyrin (TCPP), TEOS, 3-aminopropyltriethoxysilane (APTES), 3-mercaptopropyl(dimethoxy)methylsilane (MPDMMS), 1-(3-dimethylaminopropyl)-3-ethylcarbodiimide hydrochloride (EDAC), *N*-hydroxysuccinimide (NHS), and *N,N*-dimethylformamide (DMF) were purchased from Tokyo Chemical Industry (Tokyo, Japan). Ammonia water (28%) was purchased from Kishida Chemical (Osaka, Japan). Folic acid and maleimide-heterobifunctionalized polyethylene glycol (FA-PEG-Mal, M_W 3400) were purchased from Nanocs (NY, USA).

Preparation of PCSA: The preparation and structural analyses of PCSA was undertaken as described previously. In brief, APTES (15 mM) and TCPP (3.75 mM) were dissolved in DMF. EDAC (15 mM) and NHS (15 mM) were added to this solution. The mixture was stirred for 24 h at room temperature to form PCSA via the amidation reaction between the amino group of APTES and the carboxylic acid groups of TCPP.

Synthesis of ISP HNPs: IPTMS (239 µmol) and PCSA (1.7 µmol) were dissolved in 1 mL of DMF. Ammonia water (0.8 mL) was added to the above solution, which was then stirred at 100 °C for 24 h. ISP HNPs were collected by centrifugation (36 000*g*) of this dispersion and redispersed in water. This sequence was repeated thrice.

Synthesis of SP HNPs: SP HNPs were produced by a method similar to the procedure used for the synthesis of ISP HNPs by using TEOS instead of IPTMS. TEOS (239 µmol) and PCSA (1.7 µmol) were dissolved in DMF (1 mL). Ammonia water (0.8 mL) was added to the above solution, which was then stirred at 100 °C for 24 h. SP HNPs were collected by centrifugation (36 000*g*) of this dispersion and redispersed in water. This sequence was repeated thrice.

Modification of ISP HNPs with FA and PEG: ISP HNPs (12.6 mg) were dispersed in ethanol (6.5 mL). ISP HNPs were functionalized with thiol groups via the hydrolysis-condensation of MPDMMS (110 nmol) in the ISP HNPs solution with ammonia water (125 µL) at 50 °C for 24 h. The

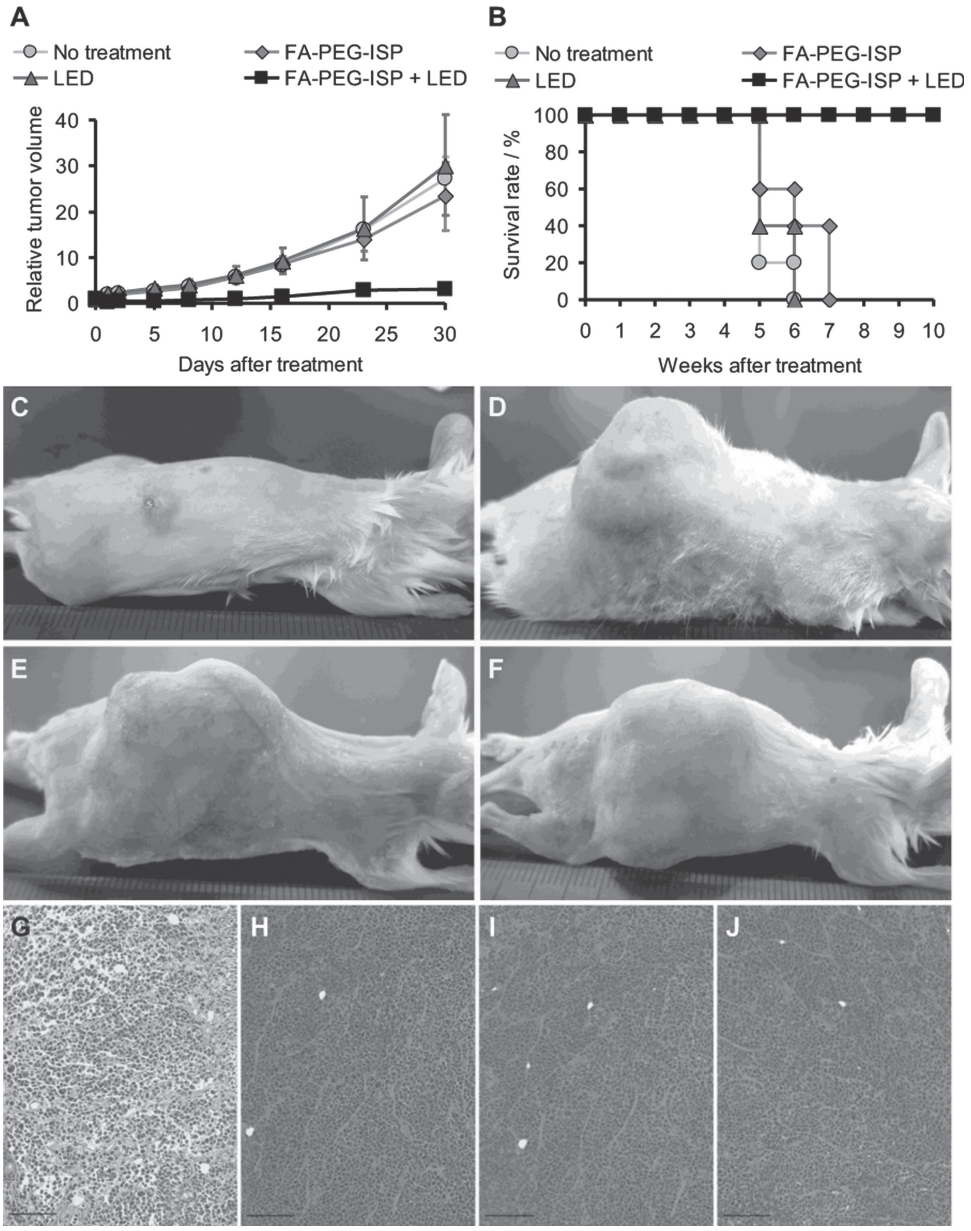

Figure 6. (A) Tumor growth behavior and (B) survival period of mice (circle: mice without treatment, diamond: mice injected with FA-PEG-ISP HNPs, triangle: mice exposed to LED light, square: mice exposed to LED light after injection of FA-PEG-ISP HNPs). Photographs of mice 30 days after treatment. Photographs of (C) mice exposed to LED light after the injection of FA-PEG-ISP HNPs, (D) mice injected with FA-PEG-ISP HNPs, (E) mice exposed to LED light, and (F) mice without treatment. (G–J) Histological observations of tumors 24 h after treatment visualized using H&E staining: scale bar 100 μm. Tumor tissue sections of (G) mice exposed to LED light after the injection of FA-PEG-ISP HNPs, (H) mice injected with FA-PEG-ISP HNPs, (I) mice exposed to LED light, (J) mice without treatment.

thiol-functionalized ISP HNPs were collected by centrifugation (36 000*g*) of this dispersion and redispersed in water. This sequence was repeated thrice. Then, ISP HNPs were modified with FA and PEG by adding FA-PEG-Mal (110 nmol) to this water containing thiol-functionalized ISP HNPs (20 mg/mL, 500 μL) and stirring at room temperature for 24 h.

Characterization: The morphology and size of the SP HNPs and ISP HNPs were studied using transmission electron microscopy (TEM) with a Hitachi H-760 machine (Hitachi, Tokyo, Japan). Solid-state ^{13}C and ^{29}Si NMR spectra of the SP HNPs and ISP HNPs were recorded with JNM-EDA600 (JEOL, Tokyo, Japan). The Fourier transform infrared spectrophotometer (FTIR) spectra were recorded with a FTIR spectrometer (Nexus 470, Nicolet, Madison, WI, USA).The compositions of the SP HNPs and ISP HNPs were analyzed by X-ray fluorescence spectroscopy (XRF, ZSX primus II, Rigaku, Tokyo, Japan). The thermal behavior of the SP HNPs and ISP HNPs were analyzed by thermogravimetric/differential thermal analysis (TG-DTA, TG/DTA 6300, Siko Instruments Inc., Chiba, Japan). The absorption bands of TCPP, SP HNPs, and ISP HNPs were measured using an ultraviolet–visible (UV-Vis) spectrophotometer (U-3000, Hitachi). The fluorescence images were obtained using the IVIS 200 Imaging System (Caliper Life Sciences, Hopkinton, MA, USA). The fluorescence intensities were estimated using the regions of interest (ROI) tool, which can determine the flux.

The hydrodynamic diameters and the zeta potentials of the ISP HNPs, SH-ISP HNRs and FA-PEG-ISP HNPs were measured in PBS (pH 7.4) using dynamic light scattering (DLS, Showa Denko, NICOMP 380 ZLS, Tokyo, Japan).

Detection of Singlet Oxygen: DPBF in ethanol solution was used as the $^1O_2$ trapping reagent. In a typical experiment, DPBF (75 nmol) and SP HNPs, ISP HNPs, or TCPP (10 μg/mL) were dissolved in ethanol (4 mL). The solution was exposed to light from an LED with a peak wavelength of 650 nm at 5 mW/cm^2 (HLV2–22RD-3W, CCS Inc., Kyoto, Japan) and a spot size of 22 mm. The absorbance of the solution at 410 nm was measured every 1 min for a 10 min period with an UV-Vis spectrophotometer. The decrease of the absorbance caused by photobleaching of DPBF was measured and corrected in all experiments. The natural logarithm values of the absorption of DPBF at 410 nm were plotted against the irradiation time and were fit by a first-order linear least-squares model to obtain the decay rate of the photosensitized process. The $^1O_2$ quantum yields of the ISP HNPs, SP HNPs, and TCPP in ethanol were calculated using Methylene Blue (MB) as the standard ($\Phi_{MB} = 0.52$ in ethanol).

Photothermal Effect in Water: SP HNPs, ISP HNPs, TCPP, and Au NRs were dissolved in water (100 μg/mL). These solutions and water were exposed to light from the LED with a peak wavelength of 650 nm at 5 mW/cm^2 and a spot size of 22 mm. The thermal images were acquired every 1 min for a 20 min period using a thermograph (Thermo Gear G100EX, NEC Avio Infrared Technologies, Tokyo, Japan), along with the temperature measurements.

Photostability Assay: SP HNPs, ISP HNPs, or TCPP were dissolved in water (100 μg/mL). The solution was exposed to the light from a LED with a peak wavelength of 650 nm at 5 mW/cm^2 and a spot size of 22 mm. The absorbance of the solution at 650 nm was measured every 5 min for a 30 min period with an UV–vis spectrophotometer.

Thiol Quantification: Quantification of the amount of thiol on the surface of SH-ISP HNPs was performed with 4-DPS. 4-DPS (1.1 mg) was dissolved in 0.1 M phosphate buffer (pH 7.0, 1 mL). SH-ISP HNPs (2.7 mg) were dispersed in 0.1 M phosphate buffer (pH 6.0, 500 μL). The 4-DPS solution (20 μL) was added to the SH-ISP HNPs suspension (500 μL). After incubatation at 30 °C for 10 min, the supernatant was collected by centrifugation (36 000*g*). The absorption spectrum of the supernatant was measured using spectrophotometer (NanoDrop ND-1000, NanoDrop Technologies, Inc., DE, USA). The amount of thiol on the surface of SH-ISP HNPs was estimated using the following equation:

$$c_{SH} = A_{324}/(\varepsilon_{324} L m),$$

where c_{SH} is the amount of thiol per gram of SH-ISP HNPs (mol/g), A_{324} is the absorbance the supernatant at 324 nm, ε_{324} is the molar absorbance coefficient of 4-TP at 324 nm (19 800 M^{-1}cm^{-1}), L is the light path (0.1 cm) and m is the concentration of SH-ISP HNPs (5.42 g/L).

FA Quantification: The amount of FA grafted on the surface of FA-PEG-ISP HNPs was estimated from A_{283} due to p-aminobenzoic acid of FA, by calibration curve method. The calibration curve was prepared by measuring the A_{283} of the solutions of FA in PBS (2.3, 11, 23, 113 and 227 nmol/mL) using spectrophotometer (NanoDrop ND-1000, NanoDrop Technologies, Inc., DE, USA). The FA-PEG-ISP HNPs were dispersed in PBS (2.7 mg/mL), and the A_{283} of this solution was measured using spectrophotometer. The amount of FA grafted on the surface of FA-PEG-ISP HNPs was estimated by substituting the A_{283} of the FA-PEG-ISP HNPs solution into the equation of the calibration curve.

Cell Line: Human myeloma cell line, RPMI 8226, was obtained from the Japanese Cancer Research Resources Bank (Tokyo, Japan). The cells were cultured in RPMI 1640 medium supplemented with 10% fetal bovine serum, 100 U/mL penicillin, and 100 μg/mL streptomycin. Before inoculation into mice, the cells were washed and resuspended in sterile PBS at a concentration of 1×10^8 cells/mL.

Ethics Statement: The study protocol was approved by the Animal Care and Use Committee of the University of Tokushima (Tokushima, Japan).

Animals: Female CB17/Icr-*Prkdc scid* mice aged 4 weeks were purchased from Charles River Laboratories Inc. (Yokohama, Japan) and were maintained in a specific pathogen-free facility in our Animal Resources Center. All experiments were approved by the Committee on Animals of the University of Tokushima. To eradicate residual natural killer (NK) cells, the mice were injected intraperitoneally with 10 μL of rabbit anti-asialo GM1 antiserum (Wako Chemicals, Osaka, Japan) one day before the tumor inoculation. The inoculation of the human myeloma cells (5×10^6 cells) was accomplished by subcutaneous injection into the backs of mice.

In vivo Fluorescence Imaging: FA-PEG-ISP HNPs (10 mg/kg) were injected intravenously into the tumor-bearing mice. In vivo fluorescence images of the mice were obtained using the IVIS Image System at λ_{ex} = 640 nm and λ_{em} = 720 nm preinjection and 1 h, 6 h, and 18 h post-injection ($n = 3$).

PDT/PTT Combination Treatment: PDT/PTT experiments were carried out on mice with tumors of diameter 250 mm^3. Tumor volumes were calculated from the formula

$$V = AB^2\pi/6,$$

where A is the longer and B is the shorter lateral diameter of the tumor. The mice were divided into four groups ($n = 5$ per cohort) as follows: those that did not receive any treatment; those to which FA-PEG-ISP HNPs (10 mg/kg) was administered; those exposed to light from a LED with a peak wavelength of 650 nm at 5 mW/cm^2 and a spot size of 22 mm for 20 min (6 J/cm^2); and those exposed to light from the LED for 20 min, 24 h after administration of the FA-PEG-ISP HNPs (10 mg/kg). Treatments were carried out once a day as soon as the tumor reached a diameter of 100 mm^3. The mice were sacrificed when the diameter of the tumor reached 3000 mm^3.

Supporting Information

Supporting Information is available from the Wiley Online Library or from the author.

Acknowledgements

This work was supported in part by Grant-in-Aid for Young Scientists (B) (24760551) from the Ministry of Education, Science, Sports, and Culture of Japan.

Received: May 23, 2013
Revised: June 27, 2013
Published online: August 19, 2013

[1] J. U. Menon, P. Jadeja, P. Tambe, K. Vu, B. Yuan, K. T. Nguyen, *Theranostics* **2013**, *3*, 152.
[2] P. Agostinis, K. Berg, K. A. Cengel, T. H. Foster, A. W. Girotti, S. O. Gollnick, S. M. Hahn, M. R. Hamblin, A. Juzeniene, D. Kessel, M. Korbelik, J. Moan, P. Mroz, D. Nowis, J. Piette, B. C. Wilson, J. Golab, *Cancer J. Clin.* **2011**, *61*, 250.
[3] L. C. Kennedy, L. R. Bickford, N. A. Lewinski, A. J. Coughlin, Y. Hu, E.S. Day, J. L. West, R. A. Drezek, *Small* **2011**, *7*, 169.
[4] Y. Hongying, W. Fuyuan, Z. Zhiyi, *Dyes Pigment* **1999**, *43*, 109.
[5] T. M. Sitnikl, J. A. Hampton, B. W. Henderson, *Br. J. Cancer* **1998**, *77*, 1386.
[6] I. J. Macdonald, T. J. Dougherty, *J. Porphyr. Phthalocyanines* **2001**, *5*, 105.
[7] M. Höckel, P. Vaupel, *J. Natl. Cancer Inst.* **2001**, *93*, 266.
[8] J. B. Mitchell, S. McPherson, W. DeGraff, J. Gamson, A. Zabell, A. Russo, *Cancer Res.* **1985**, *45*, 2008.

[9] B. W. Henderson, V. H. Fingar, *Cancer Res.* **1987**, *47*, 3110.
[10] L. E. Gerweck, *Radiat. Res.* **1977**, *70*, 224.
[11] A. Yuan, J. Wu, X. Tang, L. Zhao, F. Xu, Y. Hu, *J. Pharm. Sci.* **2013**, *102*, 6.
[12] S. Wang, P. Huang, L. Nie, R. Xing, D. Liu, Z. Wang, J. Lin, S. Chen, G. Niu, G. Lu, X. Chen, *Adv. Mater.* **2013**, DOI: 10.1002/adma.201204623.
[13] B. Jang, J.-Y. Park, C.-H. Tung, I.-H. Kim, Y. Choi, *ACS Nano* **2011**, *5*, 1086.
[14] Y. Zhang, J. F. Lovell, *Theranostics* **2012**, *2*, 905.
[15] L. B. Josefsen, R. W. Boyle, *Theranostics* **2012**, *2*, 916.
[16] M. Ethirajan, Y. Chen, P. Joshi, R. K. Pandey, *Chem. Soc. Rev.* **2011**, *40*, 340.
[17] J. He, Z. Wei, L. Wang, Z. Tomova, T. Babu, C. Wang, X. Han, J. T. Fourkas, Z. Nie, *Angew. Chem. Int. Ed.* **2013**, *52*, 2463.
[18] S. Link, C. Burda, M. B. Mohamed, B. Nikoobakht, M. A. El-Sayed, *J. Phys. Chem. A* **1999**, *103*, 1165.
[19] S. Link, Z. L. Wang, M. A. El-Sayed, *J. Phys. Chem. B* **2000**, *104*, 7867.
[20] S.-K. Lee, I. Okura, *Analyst* **1997**, *122*, 81.
[21] S.-K. Lee, I. Okura, *Anal. Chim. Acta* **1997**, *342*, 181.
[22] T. Itoh, K. Yano, Y. Inada, Y. Fukushima, *J. Am. Chem. Soc.* **2002**, *124*, 13437.
[23] A. Kearvell, F. Wilkinson, *Mol. Cryst.* **1968**, *4*, 69.
[24] S. Kim, T. Y. Ohulchanskyy, D. Bharali, Y. Chen, R. K. Pandey, P. N. Prasad, *J. Phys. Chem. C* **2009**, *113*, 12641.
[25] C. S. Jin, J. F. Lovell, J. Chen, G. Zheng, *ACS Nano* **2013**, *7*, 2541.
[26] J. F. Lovell, C. S. Jin, E. Huynh, H. Jin, C. Kim, J. L. Rubinstein, W. C. W. Chan, W. Cao, L. V. Wang, G. Zheng, *Nat. Mater.* **2011**, *10*, 324.
[27] P. Couleaud, V. Morosini, C. Frochot, S. Richeter, L. Raehm, J.-O. Durand, *Nanoscale* **2010**, *2*, 1083.
[28] Material Safety Data Sheet Docusate sodium, http://www.sciencelab.com/msds.php?msdsId=9923877.
[29] L. M. Rossi, P. R. Silva, L. L. R. Vono, A. U. Fernandes, D. B. Tada, M. S. Baptista, *Langmuir* **2008**, *24*, 12534.
[30] T. Y. Ohulchanskyy, I. Roy, L. N. Goswami, Y. Chen, E. J. Bergey, R. K. Pandey, A. R. Oseroff, P. N. Prasad, *Nano Lett.* **2007**, *7*, 2835.
[31] K. Hayashi, M. Nakamura, H. Miki, S. Ozaki, M. Abe, T. Matsumoto, K. Ishimura, *Adv. Funct. Mater.* **2012**, *22*, 3539.
[32] K. Hayashi, M. Nakamura, H. Miki, S. Ozaki, M. Abe, T. Matsumoto, K. Ishimura, *Chem. Commun.* **2013**, *49*, 5334.
[33] K. Hayashi, M. Nakamura, K. Ishimura, *Chem. Commun.* **2012**, *48*, 3830.
[34] K. Hayashi, M. Nakamura, K. Ishimura, *Adv. Healthcare Mater.* **2012**, *2*, 756.
[35] S. Ek, E. I. Iiskola, L. Niinistö, J. Vaittinen, T. T. Pakkanen, A. Root, *J. Phys. Chem. B* **2004**, *108*, 11454.
[36] A. S. Maria Chong, X. S. Zhao, *J. Phys. Chem. B* **2003**, *107*, 12650.
[37] Y. Gao, N. R. Choudhury, N. Dutta, J. Matisons, M. Reading, L. Delmotte, *Chem. Mater.* **2001**, *13*, 3644.
[38] R. Rahimi, F. Moharrami, S. H. Rahmanpor, *Asian J. Chem.* **2010**, *22*, 4398.
[39] R. M. Silverstein, F. X. Webster, D. J. Kiemle, *Spectrometric Identification of Organic Compounds*, 7th Ed., John Wiley & Sons, New York **2005**.
[40] Z. Zhang, A. L. Verma, M. Yoneyama, K. Nakashima, K. Iriyama, Y. Ozaki, *Langmuir* **1997**, *13*, 4422.
[41] M. Zaharescu, A. Jitianu, A. Braileanu, J. Madarász, G. Pokol, *J. Therm. Anal. Calorim.* **2001**, *64*, 689.
[42] N. Primeau, C. Vautey, M. Langlet, *Thin Solid Films* **1997**, *310*, 47.
[43] A. Fidalgo, L. M. Ilharco, *J. Non-Cryst. Solids* **2001**, *283*, 144.
[44] E. José Nassar, K. J. Ciuffi, S. J. L. Ribeiro, Y. Messaddeq, *Mater. Res.* **2003**, *6*, 557.
[45] C.-Y. Kim, A-R. Jang, B.-I. Kim, D.-H. Suh, *J. Sol-Gel Sci. Technol.* **2008**, *48*, 336.
[46] E. Enríquez, J.F. Fernández, M.A. de la Rubia, *Carbon* **2012**, *50*, 4409.
[47] L. Xiao, L. Gu, S. B. Howell, M. J. Sailor, *ACS Nano* **2011**, *5*, 3651.
[48] R. W. Redmond, J. N. Gamlin, *Photochem. Photobiol.* **1999**, *70*, 391.
[49] P. Nowak-Sliwinska, A. Karocki, M. Elas, A. Pawlak, G. Stochel, K. Urbanska, *Biochem. Biophys. Res. Commun.* **2006**, *349*, 549.
[50] C. Hadjur, N. Lange, J. Rebstein, P. Monnier, H. van den Bergh, G. Wagnières, *J. Photochem. Photobiol. B-Biol.* **1998**, *45*, 170.
[51] J. M. Fernandez, M. D. Bilgin, L. I. Grossweiner, *J. Photochem. Photobiol. B-Biol.* **1997**, *37*, 131.
[52] J. M. Harris, R. B. Chess, *Nat. Rev. Drug. Discov.* **2003**, *2*, 214.
[53] H. Maeda, J. Wu, T. Sawa, Y. Matsumura, K. Hori, *J. Control Release* **2000**, *65*, 271.
[54] M. K. Yu, J. Park, S. Jon, *Theranostics* **2012**, *2*, 3.
[55] C. K. Riener, G. Kada, H. J. Gruber, *Anal. Bioanal. Chem.* **2002**, *373*, 266.